ADVANCED HEALTHCARE MATERIALS
www.advhealthmat.de

Tissue Niche Miniature of Glioblastoma Patient Treated with Nano-Awakeners to Induce Suicide of Cancer Stem Cells

Seon-Jin Yoon, Sewoom Baek, Seung Eun Yu, Euna Jo, Dongkyu Lee, Jin-Kyoung Shim, Ran Joo Choi, Junseong Park, Ju Hyung Moon, Eui-Hyun Kim, Jong Hee Chang, Jung Bok Lee, Joon-Sang Park, Hak-Joon Sung, and Seok-Gu Kang**

Patient-specific cancer therapies can evolve by vitalizing the mother tissue-like cancer niche, cellular profile, genetic signature, and drug responsiveness. This evolution has enabled the elucidation of a key mechanism along with development of the mechanism-driven therapy. After surgical treatment, glioblastoma (GBM) patients require prompt therapy within 14 days in a patient-specific manner. Hence, this study approaches direct culture of GBM patient tissue (1 mm diameter) in a microchannel network chip. Cancer vasculature-mimetic perfusion can support the preservation of the mother tissue-like characteristic signatures and microenvironment. When Active Ingredient and radiation are administered within 1 day, the responsiveness of the tissue in the chip reflected the clinical outcomes, thereby overcoming the time-consuming process of cell and organoid culture. When the tissue chip culture is continued, the intact GBM signature gets lost, and the outward migration of stem cells from the tissue origin increases, indicating a leaving-home effect on the family dismantle. Nanovesicle production using GBM stem cells enables self-chasing of the cells that escape the Active Ingredient effect owing to quiescence. The anti-PTPRZ1 peptide display and Active Ingredient loading to nanovesicles awakes cancer stem cells from the quiescent stage to death. This study suggests a GBM clinic-driven avatar platform and mechanism-learned nanotherapy for translation.

1. Introduction

Each cancer microenvironment contains various cells, extracellular matrix (ECM) and humoral factors in heterogeneous combinations that are specific to the patient, location and stage.[1] Continuous progress has been made in the development of a cancer avatar platform to preserve the characteristic signature and microenvironment using state-of-the-art technologies such as cell spheres, organoids, and 3D printing.[2] Nonetheless, unmet needs remain to present the whole set of heterogeneous niches with associated cells, to meet the degree of urgency for each patient, and to reproduce the drug effect in perfusable microchannel circulation. In particular, the prognosis of glioblastoma (GBM) after medical treatment is dependent on the patient-specific cancer stage, genetic signature, and environmental characteristics.[3] Even its therapeutic treatment requires a rapid decision within 14 days after surgery.[4] Hence, GBM treatment options, including Active Ingredient (TMZ) and/or ir-radiation, as well as the dose, time point and

S.-J. Yoon, E. Jo, D. Lee, J.-K. Shim, R. J. Choi, J. Park, J. H. Moon, E.-H. Kim, J. H. Chang, S.-G. Kang
Department of Neurosurgery
Severance Hospital
Yonsei University College of Medicine
50-1 Yonsei-ro, Seodaemun-gu, Seoul 03722, Republic of Korea
E-mail: seokgu9@yuhs.ac

S.-J. Yoon, E. Jo, D. Lee, J.-K. Shim, R. J. Choi, E.-H. Kim, S.-G. Kang
Brain Tumor Translational Research Laboratory
Avison Biomedical Research Center
Yonsei University College of Medicine
50-1 Yonsei-ro, Seodaemun-gu, Seoul 03722, Republic of Korea

S. Baek, H.-J. Sung
Department of Brain Korea 21 FOUR Project for Medical Science
Medical Engineering
Yonsei University College of Medicine
50-1 Yonsei-ro, Seodaemun-gu, Seoul 03722, Republic of Korea
E-mail: hj72sung@yuhs.ac

S. Baek, S. E. Yu, H.-J. Sung
Department of Medical Engineering
Yonsei University College of Medicine
50-1 Yonsei-ro, Seodaemun-gu, Seoul 03722, Republic of Korea

J. Park
Precision Medicine Research Center
College of Medicine
The Catholic University of Korea
222 Banpo-daero, Seocho-gu, Seoul 06591, Republic of Korea

J. B. Lee
Department of Biological Science
Sookmyung Women's University
25, Cheongpa-ro 47ga-gil, Yongsan-gu, Seoul 04314, Republic of Korea

The ORCID identification number(s) for the author(s) of this article can be found under https://doi.org/10.1002/adhm.202201586

DOI: 10.1002/adhm.202201586

length should be decided in a speedy manner and be specific to each patient, justifying the choice of GBM as the cancer type for this study.

The present study aimed to meet these clinical demands by approaching the direct culture of GBM patient tissues with a 1 mm post-punching diameter in a 3D microchannel network chip ("GBM miniature"). The circulation of microchannel network enables the delivery of oxygen and nutrients to the entire 3D space, as the 200 μm diffusion limit can be overcome,[5] which mimics the dense and leaky features of tumor vasculature to feed aggressively growing GBM masses. The microflow allows for the re-exposure of GBM to drug effects in channel circulation.[6] The gelatin matrix body encapsulating the microchannel network enables the deployment of GBM tissue with monitoring cell migration from the tissue. As seen in the brain,[7,8] GBM cells can migrate throughout the gelatin matrix and microchannels as ground and routes, respectively, in the system.

As GBM tissue-related mechanisms can be studied in GBM miniature, mechanism-driven therapy can be proposed, representing a breakthrough point of the study. During migration from the GBM origin, cancer stem cells (CSCs) maintain the quiescent stage (G0) and thus escape the effect of TMZ, which disrupts the cell death induction by cell cycle, thereby serving as a culprit of GBM recurrence. This process is operated by the expression and activation of protein tyrosine phosphatase receptor type Z1 (PTPRZ1) on the CSC membrane. Hence, the inhibition of PTPRZ1 signaling is suggested as a promising therapy to awaken CSCs from the G0 phase into death upon exposure to TMZ. As the same cancer cell type-specific targeting was proven previously,[9] this study also utilized nanovesicles (NVs) from GBM stem cells by applying the concept of self-targeting based on spontaneous cancer cell–cell interactions observed in the growing tumor mass. CSC-NVs were designed to display anti-PTPRZ1 peptides and to load TMZ so that migratory CSCs can be chased, awakened, and induced to die through unprecedented functional programing.

2. Results

2.1. Justification to Use GBM Miniature for a Patient-Specific Therapy

The GBM miniature was used as a patient-specific platform to enable prompt drug screening for early treatment, thereby improving the survival rate (**Figure 1**a). GBM treatment should be patient-specific with respect to progression stage, genetic profile, and microenvironment.[3] Hence, the GBM miniature was designed to culture patient tissue pieces directly in the microchannel network chip under perfusion so that these patient-specific factors could be preserved. Therefore, prompt screening of treatment options after surgery can enhance survival rates.[4] The production process of the GBM miniature started from obtaining biopsied tissue (mother tissue) from the tumor mass through surgery, followed by punching the tissue into pieces (≈1 mm diameter) (Figure 1b). A polydimethylsiloxane (PDMS) mold was cast using a 3D-printed polylactic acid (PLA) structure, and Poly(N-isopropylacrylamide (PNIPAM) threads were inserted into the mold. Variations of PNIPAM concentration (50–53%) resulted in control of the diameter, and the 53% concentration was determined due to the minimized bubble formation and the microvasculature-mimetic fiber diameter (average 16 μm) (Figure S1a, Supporting Information). According to a clinical report,[1a,10] CSCs migrate through the microvasculature and neuronal networks. Therefore, the size distribution of the PNIPAM fibers was determined to mimic that of the microvasculature, which enabled the microchannel to facilitate CSC invasion in the GBM miniature.

The GBM tissue piece was embedded in a gelatin gel before crosslinking, and the gel tissue was positioned into a PDMS mold with PNIPAM threads, followed by microbial transglutaminase (mTG) crosslinking of the gel. The gel concentration was determined to 5.5%, as previously reported.[5b] The gelatin gel provided a foundation for 3D tissue culture by enabling the formation of a perfusable channel network, which facilitates cancer cell migration with drug delivery into the tissue in the GBM miniature. PNIPAM dissolved away upon a temperature shift below 32 °C with perfusion washing, thereby generating channel networks in the crosslinked gel with the GBM tissue (Movie S1, Supporting Information). Channel perfusion was confirmed by perfusion staining of fluorescence microbeads (Figure S1b, Supporting Information), which made the GBM miniature ready for culture with medium perfusion. As the mother tissues were preserved for further studies, they were cryopreserved, resulting in no significant loss of cell viability after storage for 1 year (Figure S2, Supporting Information).

Because the GBM miniature functioned as a niche reservoir to decide a patient-specific therapy, the function was compared among the test groups, including 2D tissue culture polystyrene (2D TCPS) and 3D systems with a gel base (static without channel) and the addition of channel (static with channel) and channel perfusion (GBM miniature), so that the incremental benefits from 2D to 3D and further to the addition of channel and perfusion could be revealed (Figure S3, Supporting Information). The tissue viability increased significantly from day 1 to 7 only in the GBM miniature as opposed to the other culture systems (**Figure 2**a), indicating a synergistic benefit of the cooperation among 3D gelatin gel, channel network and perfusion. In our previous study,[5b] the advantages of perfusion in the channel network were demonstrated with respect to improving the viability of GBM tissue and facilitating drug delivery into the GBM tissue. In the clinical setting, standard treatment for GBM must start within 14–21 days after surgical removal of tumor masses, alerting a time-sensitive decision of patient-specific drug choice (Figure 2b). As a widely accepted test control in current research, patient-specific drug screening with cell spheres (CS) usually takes more than 30 days, owing to the lengthy process of cell isolation and culture. In contrast, the GBM miniature was designed to enable drug screening in one day, representing an unprecedented advantage for precision medicine. The preparation of the GBM

J.-S. Park
Department of Computer Engineering
Hongik University
94, Wausan-ro, Mapo-gu, Seoul 04066, Republic of Korea
S.-G. Kang
Department of Medical Science
Yonsei University Graduate School
Seoul 03722, Republic of Korea

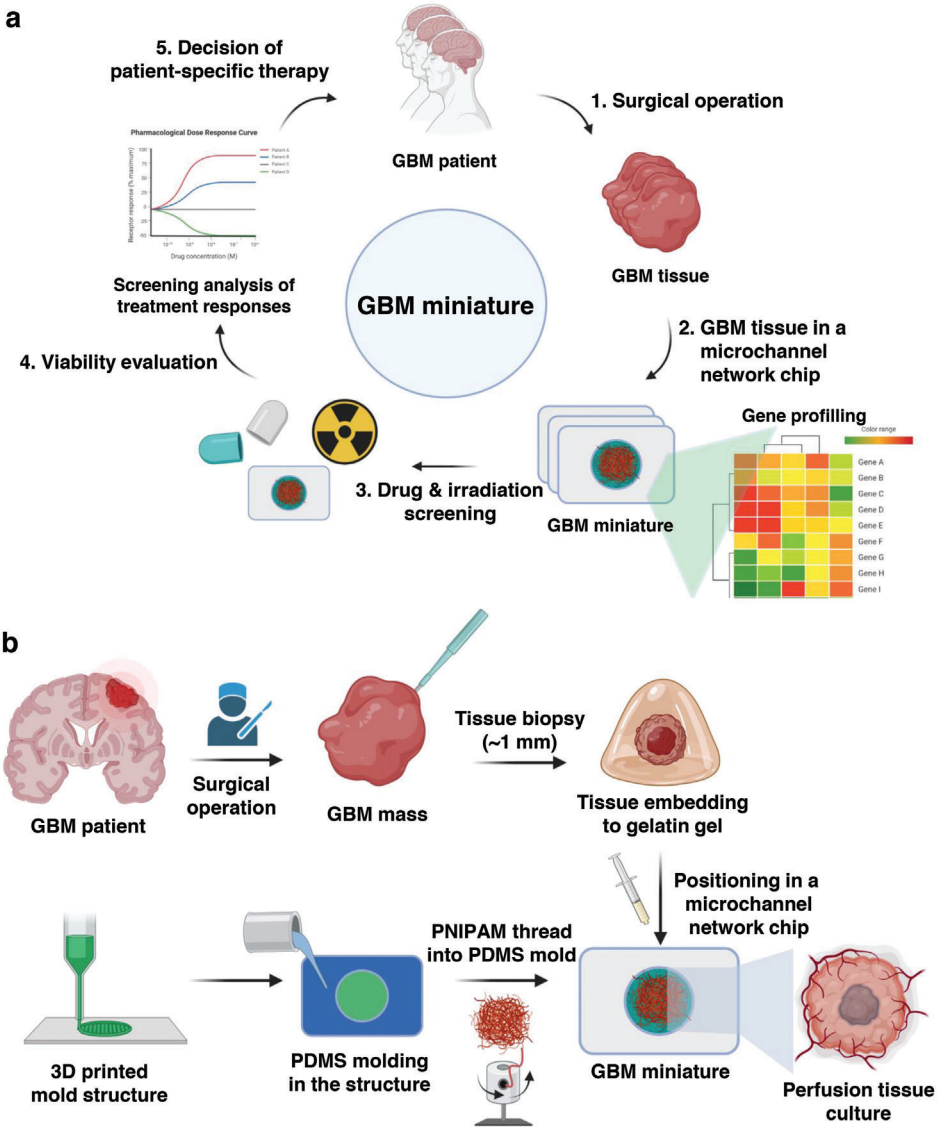

Figure 1. Utility and development process of GBM miniature. a) Overview of the GBM miniature approach as a patient-specific platform to enable prompt drug screening and early treatment, thereby improving the survival rate. b) The production procedure of the GBM miniature starts with obtaining biopsied tissues from tumor masses via surgery, followed by punching the tissues into pieces (≈1 mm diameter). Simultaneously, a PDMS mold is casted using a 3D-printed PLA structure, followed by the insertion of PNIPAM threads in the mold. The GBM tissue piece is then embedded in a gelatin gel before crosslinking. The gel-tissue is positioned into the PDMS mold with the PNIPAM threads, followed by mTG crosslinking of the gel. PNIPAM dissolved upon a temperature shift below 32 °C with perfusion washing, thus generating channel networks in the crosslinked gel with the GBM tissue. This process makes the GBM miniature ready for culture with medium perfusion.

miniature took a total of 6 h including 5-h chip process with 1 h period of tissue embedding. When the call was received to provide GBM tissues from the operation side, the chip was prepared for 5 h before tissue delivery, and tissue embedding took 1 h.

Indeed, the GBM miniature (n = 157) exhibited an 86% culture success rate compared to the nearly 50% failure of the CS culture (n = 222) (Figure 2c), which represents a significant advance in the preservation of surgically removed samples for mining patient data. The time-dependent incremental losses of genetic signatures as an indication of cell composition were analyzed in GBM samples by RNA sequencing (Figure 2d). The GBM miniature mice maintained the signatures of all cell types from the mother tissue within the 1-day screening period. During the entire culture period, GBM maintenance appeared to be superior to that of the CS culture, which incrementally lost most signatures, except that of neural progenitor-like cells, until 30 days of screening. These results emphasize the punchline advantage of the GBM miniature to present the genetic and cell signatures of each mother tissue from the corresponding patient within the drug screening period. Upon further culture for 21 days, the GBM miniature robustly preserved the signatures of the mother tissue (100–67%), indicating a significant utility for long-term or delayed drug screening according to the status of each patient (Figure S4, Supporting Information).

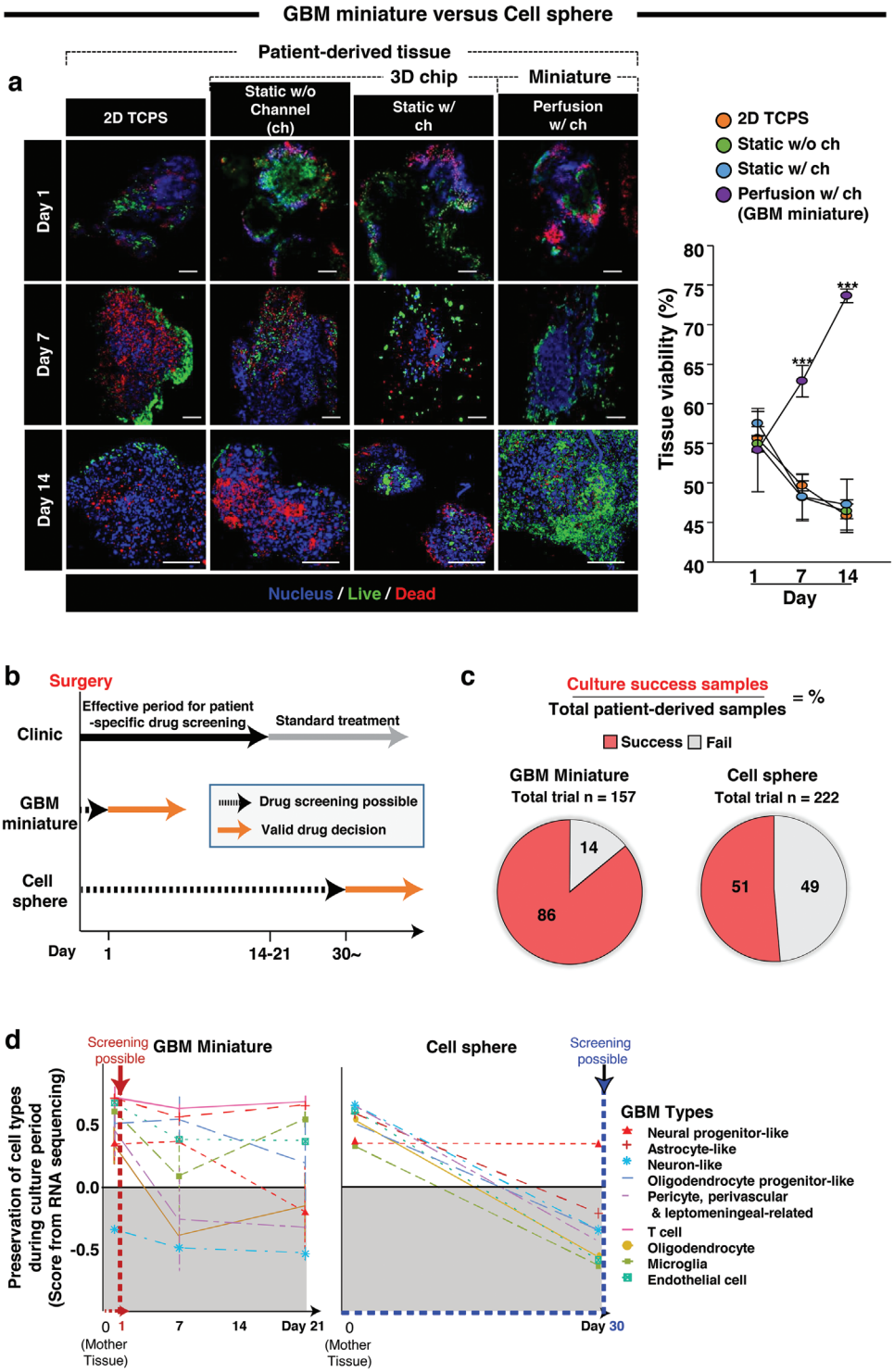

Figure 2. GBM miniature as a niche reservoir to decide a patient-specific therapy. Perfusion culture of GBM patient tissue (≈1 mm diameter) in a microchannel network chip was defined as a GBM miniature. a) The tissue viability (live-green, dead-red, and blue-nucleus) increased significantly from day 1 to 7 in only the GBM miniature, but not in the other culture systems, indicating a synergistic benefit of the cooperation among 3D gelatin gel, channel network and medium perfusion ($n = 3$, scale bar = 100 μm). b) In clinical setting, standard GBM treatment must start within 14–21 days after surgical operation to remove tumor masses. As a widely accepted test control in the current research, patient-specific drug screening using cell sphere (CS) usually takes more than 30 days owing to the lengthy process of cell isolation and culture. In contrast, the GBM miniature enables completion of drug screening in ≈1 day, representing an unprecedented advantage to decide a patient-specific therapy. c) When calculated following the equation, the GBM miniature exhibited 88% of culture success rate, compared to the nearly 50% failure of cell sphere culture, representing a significant advance in the preservation of clinic-derived samples for patient data mining. d) The time-dependent changes in the genetic signatures of cell composition were

2.2. GBM Miniature as a Prompt Drug Screening Toolbox

The GBM miniature was developed to meet the clinical needs for early treatment by prompt drug screening. When GBM clinical data were analyzed to define the need for rapid decision making and treatment (**Figure 3**a), TMZ treatment before 15 days after surgery maintained a high survival rate (over 60% in 19 patients) for 60 months. In contrast, when treatment was performed 15 days post-surgery, the survival rate ($n = 100$ patients) decreased to <50% at 20 months and continuously decreased to ≈10% at 60 months. A major reason for this marked difference in prognosis between treatment before and 15 days after surgery was identified from clinical MRI imaging with gadolinium as a contrast agent (Figure 3b). The brain of a drug-working case exhibited pointed GBM masses in arrested patterns, indicating efficient suppression of GBM cell migration and consequent tumor spreading. In contrast, a drug-escaping case showed diffusive GBM masses in migratory patterns as a clear indication of tumor spreading and increased mortality.

Hence, the GBM miniature was designed to culture a mother tissue piece directly in a channel network chip under perfusion so that patient-specific screening of therapeutics can be performed rapidly to allow for early treatment and improve the survival rate (Figure 3c). As a validation of the utility (Figure 3d), the cell viability results from live/dead assays revealed that the GBM miniature effectively captured the potent anticancer effects of TMZ or irradiation treatment compared with those of phosphate buffered saline (PBS) or vehicle (dimethyl sulfoxide) treatment. GBM miniature cells reflected the anticancer effects of TMZ or irradiation treatment more sensitively than the CS culture, according to the quantitative analysis results of cell viability (Figure 3e). As these responses were achieved on day 1 post-culture, the GBM miniature is suggested as an unprecedented platform for prompt drug decisions and early treatment.

2.3. Migration of GBM Stem Cells from the Tissue of Origin

As a major method to escape the effects of TMZ, GBM stem cells maintain a quiescent status and then migrate from the corresponding tumor mass, serving as a culprit of tumor spread and recurrence. The RNA sequencing results indicated patient-dependent outward migration patterns of neuro-like (patients 1–2), astrocyte-like (patients 3–4), and both GBM types (patients 5–8) from each tissue origin for 14–21 days in the miniatures (**Figure 4**a). In patients 1–4, the other cell types did not show clear migration patterns during that period, likely owing to patient-dependent differences in migratory cell composition. As the preservation of mother tissue-like signatures by GBM miniature cells was validated up to 21 days post-culture (Figure S4, Supporting Information), the migratory cells were characterized at day 21 by immunostaining and then collected daily until day 28 for the analysis of marker expression in the post-migration cell population (Figure 4b).

Because microchannels (yellow) appeared to facilitate the migration of these cells as routes to invade the outward areas from the tissue origin, migrating cells around the microchannels were characterized at day 21 post-culture (Figure 4c). These cells were positive for CSC markers (CD133 and Oct3/4), oligodendrocyte markers (Olig2) and glial markers (GFAP), and the microchannels promoted the migration of these cells significantly, as the distance was quantitatively analyzed. According to FACS analysis of marker expression in the migrated cells post-harvest daily from days 21 to 28, most cells were migratory ($PTPRZ1^+$ for 90.4%) and had dominant CSC characteristics ($CD133^+/Oct3/4^+$ for 60.3%), with partial commitment to GBM cells ($Oligo2^+/GFAP^+$ for 45.6%) (Figure 4d and Figure S5, Supporting Information). These results indicated that outward cell migration from the GBM mass was critically associated with PTPRZ1, and CSCs migrated before and after their complete transformation to GBM characteristics. The commitment of CSCs to GBM cells has been observed in the recurrence process.

2.4. Nano-Awakener to Target and Eliminate Migratory CSCs

CSCs migrate in an adherent fashion from the GBM mass and thereby escape the effect of TMZ, thus surviving and recurring, which directs the design of nano-awakeners to target and eliminate migratory CSCs (**Figure 5**a). The GBM miniature allowed for cell migration from the tissue of origin; thus, migrated cells were harvested and sorted to select CSCs, followed by serial filtering to produce CSC-NVs. Because PTPRZ1 plays a key role in promoting quiescent CSC migration by maintaining cell adherence, its targeting peptide (PT-PEG) was displayed in the form of CSC-NV-PT-PEG through step-by-step conjugation using a scramble peptide (SC-PEG) as a control (Figure S6a, Supporting Information). TMZ was then loaded to produce a nano-awakener (CSC-NV-PT-TMZ) so that migratory $PTPRZ^+$ CSCs could be chased and awakened to death via unprecedented therapeutic action to suppress quiescence and attachment simultaneously.

The targeting peptide PT sequence was set to exert sufficient binding efficiency to block PTPRZ, as simulated by computer 3D-modeling with the best docking score (−9.513) (Figure 5b). Incremental TMZ loading to produce nano-awakeners (>1 μg TMZ) was confirmed using LC-MS/MS, and the NV sizes before and after PT-PEG display to nano-awakeners (average ≈117 nm) were compared to the control NV without or with SC-PEG display using transmission electron microscopy (TEM) imaging (Figure 5c and Figure S6b,c, Supporting Information). PT-displayed CSC-NVs exhibited superior targeting efficiency compared to liposomes and SC or no-peptide CSC-NVs, as indicated by co-localization with PTTRZ1 in CSCs (Figure 5d). The nano-awakener with additional TMZ treatment in the media exerted the most effective anticancer effect on CSCs compared to no TMZ (CSC-NV-PT-PEG) and only TMZ loading (nano-awakener) (Figure 5e). This result indicated that TMZ loading

analyzed in GBM samples ($n = 9$) by RNA sequencing. The GBM miniature maintained the signatures of mother tissue-originated cell types for the possible period of screening (1 day). During the entire culture period, the GBM miniature appeared to be superior to cell spheres, which incrementally lost the signatures of most cells except neural progenitor-like cells, until the end of the possible period of screening (30 days). The RNA sequencing-scores were normalized by log2-transforming the count-data. Data = mean ± standard deviation. $***p < 0.001$ versus the other test groups.

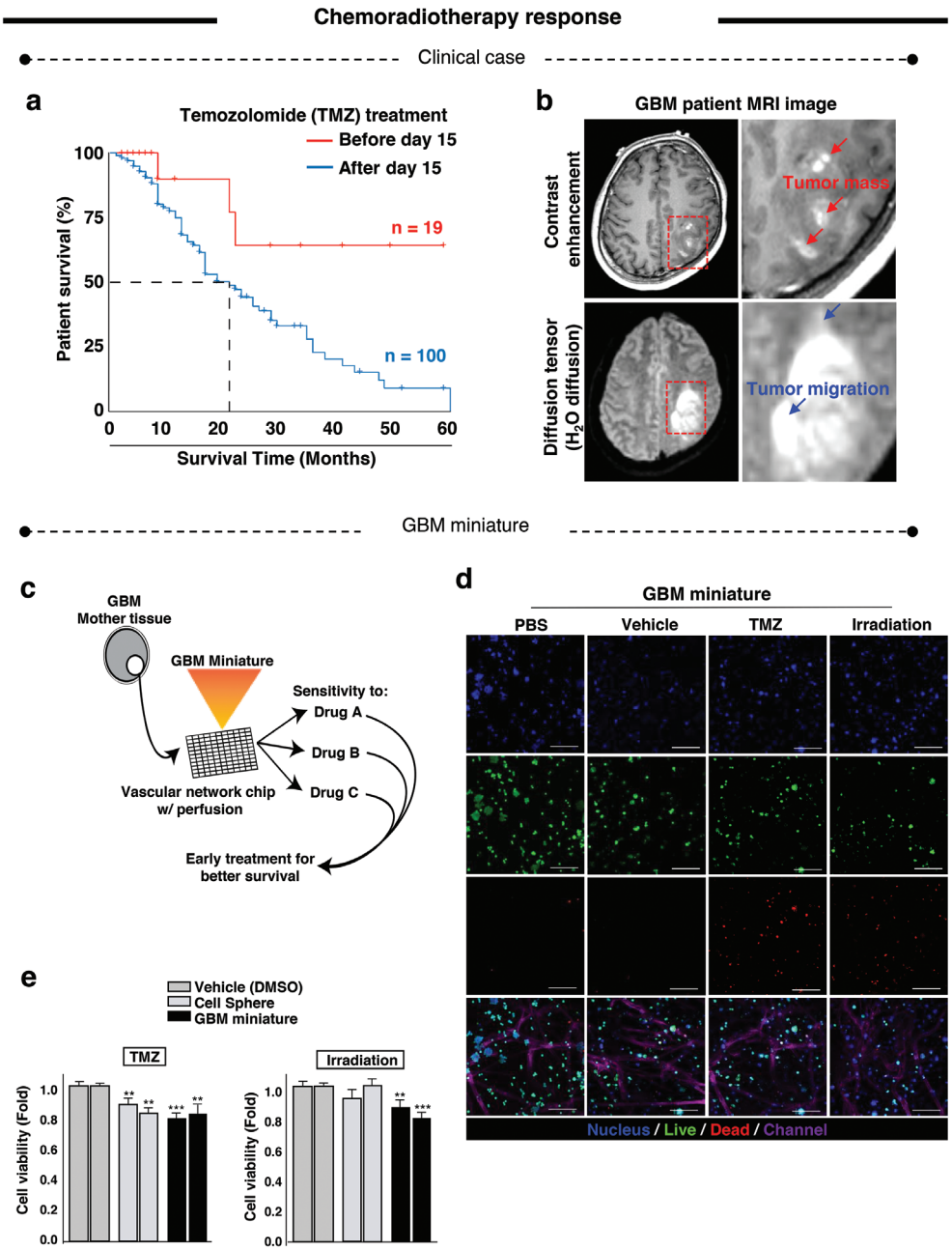

Figure 3. GBM miniature as a prompt drug screening toolbox to meet the clinical need for early treatment. a) In clinical GBM samples, TMZ treatment before 15 days post-surgery maintained a high survival rate (over 60% in 19 patients) for 60 months. In contrast, when the treatment was performed on day 15 post-surgery, the survival rate (n = 100 patients) decreased below 50% at 20 months and continuously decreased to ≈10% at 60 months. b) MRI imaging of GBM patients using a gadolinium contrast agent revealed that the brain of a drug-working case (top) exhibited pointed GBM masses (red-box) in arrested patterns (red-arrow, magnified). In contrast, a drug-escaping case (bottom) showed diffusive GBM masses (red-box) in migratory patterns (blue-arrow, magnified). c) The GBM miniature is designed to culture a mother tissue piece in a channel network chip so that patient-specific screening of therapeutics can be completed rapidly to allow early treatment and improve the survival rate. d) Live/dead assays for cell viability at day 1 post-culture showed that the GBM miniature effectively captured the potent anticancer effects of TMZ or irradiation treatment compared with those of PBS or vehicle (DMSO) treatment (n = 3, scale bar = 200 μm). e) Quantitative analysis of cell viability revealed that the GBM miniature reflected the anticancer effects of TMZ or irradiation treatment more sensitively within 1-day post-culture than the cell sphere culture (n = 3). The percentage values of cell viability were normalized to that of the vehicle (fold change). Data = mean ± standard deviation, $^{**}p$ <0.01, $^{***}p$ < 0.001 versus vehicle.

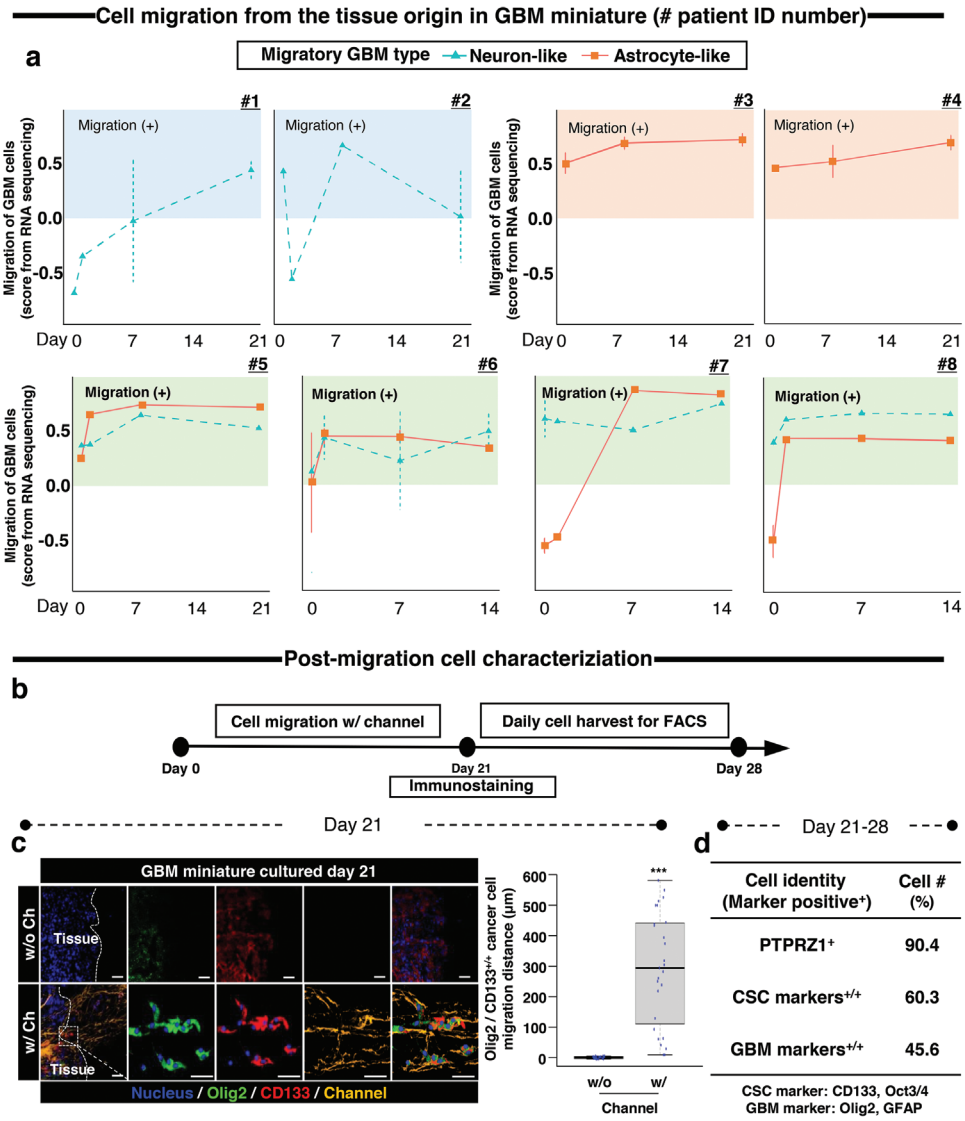

Figure 4. Migration of GBM stem cells from the tissue origin in the miniature. a) RNA sequencing results indicate patient-dependent outward migration patterns of neuro-like (cyan, patient 1–2), astrocyte-like (orange, patient 3–4), and both GBM types (patient 5–8) from each tissue origin for 14–21 days in the miniature culture. In patient 1–4, the other cell type did not show clear migration patterns in that period. The RNA sequencing scores were normalized by log2-transforming the count-data. b) As illustrated, GBM cells that migrated along the microchannel were subjected to immunostaining (day 21), and the migrated cells were collected daily for FACS analysis (day 22–28). c) Microchannels (yellow) served as a route for GBM stem cells (blue-nucleus/green-Oligo2+/red-CD133+) to migrate outward from the original tissue compared with the without channel group ($n = 3$, scale bar = 50 μm), which was supported by quantitative analysis. Data = mean ± standard deviation ***$p < 0.001$ versus the without channel group. d) When migrated cells were harvested from day 21 to 28 post-culture, the FACS analysis results showed that most cells were migratory (PTPRZ1$^+$ for 90.4%) and had dominant stem cell characteristics (CD133$^+$/Oct3/4$^+$ for 60.3%) with partial commitment to GBM lineage (Oligo2$^+$/GFAP$^+$ for 45.6%).

alone could not sufficiently induce CSC death but triggered CSCs to be more susceptible to extra treatment with soluble TMZ.

2.5. Pro-TMZ Effects of Nano-Awakener against CSCs

The pro-TMZ effects of the nano-awakener against CSCs were further examined to validate whether the therapeutic mechanism suppressed CSC attachment with activation of the S-phase process. Fetal bovine serum (FBS) is typically used to promote cell attachment in in vitro culture. FBS (10%) promoted CSC attachment from the suspension in a 3-day culture but attenuated the resetting of the suspension status when the concentration of CSC-NV-PT-PEG (nano-awakener without TMZ loading) was increased to 160 μg mL^{-1} (**Figure 6**a and Figure S7a,b, Supporting Information). As a result, cell spreading decreases, thus reducing CSC viability. Nano-awakeners are programmed to activate the S-phase process in quiescent CSCs, thereby inducing susceptibility to TMZ treatment. Hence, CSCs were isolated from three cases (1–3) of miniature GBM using patient samples (Figure 6b). Indeed, treatment with CSC-WT-PT-PEG during the 3-day culture induced the S-phase process (2–6 times), making CSCs

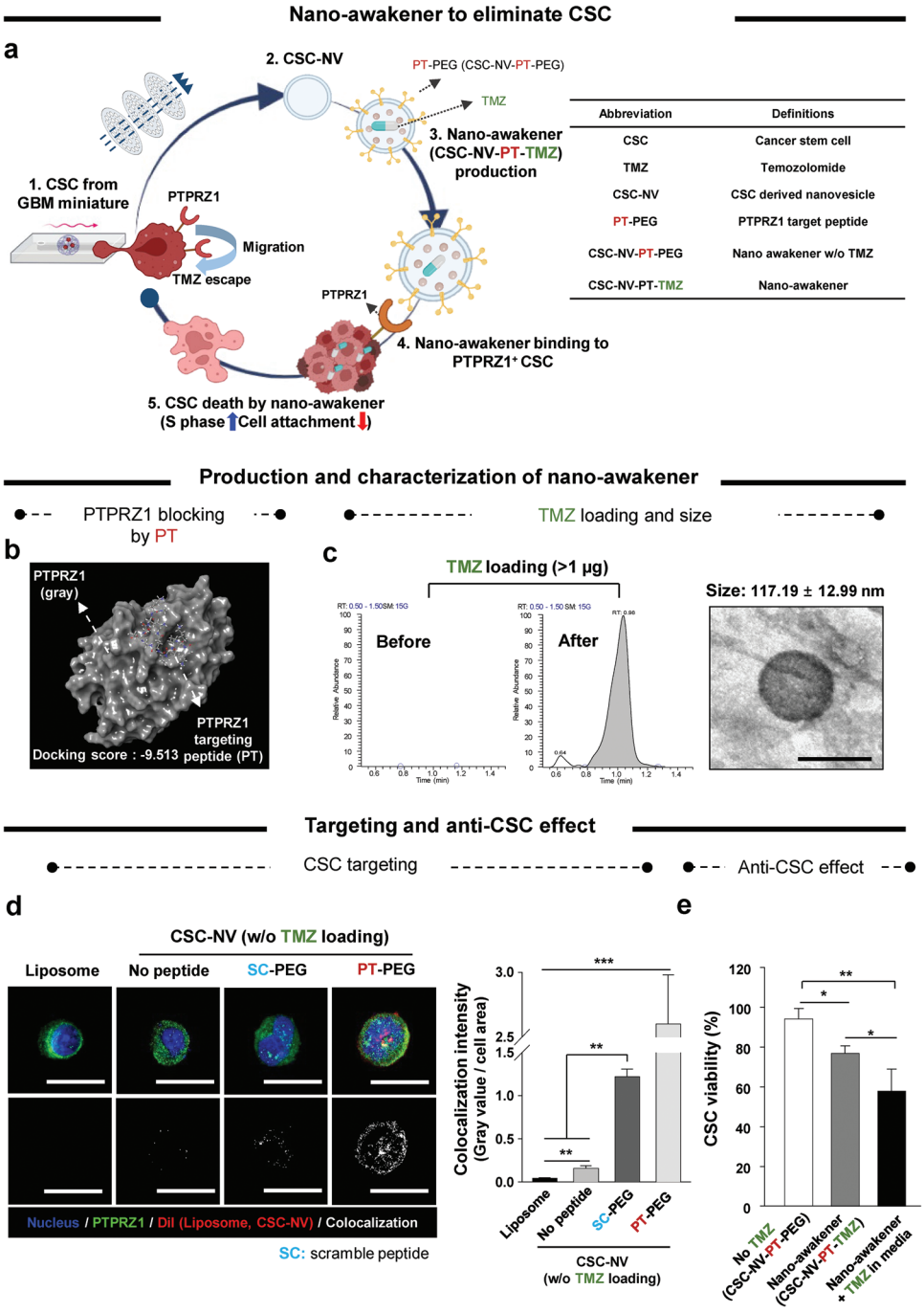

Figure 5. Nano-awakener to target and eliminate migratory CSCs escaping from the effect of TMZ. a) CSCs migrate in an adherent fashion from the GBM mass and escape the effect of TMZ for survival and recurrence. Hence, CSCs from GBM were harvested and subjected to serial filtering to produce CSC-NV. Next, a PTPRZ1-targeting peptide (PT-PEG) was displayed in the form of CSC-NV-PT-PEG, followed by TMZ loading to produce a nano-awakener (CSC-NV-PT-TMZ). As a result, an unprecedented therapeutic action was programmed to chase and awake migratory PTPRZ^{+} CSCs to activate the S phase process and suppress cell attachment so that TMZ could eliminate CSCs effectively. b) The binding efficiency of PT in blocking PTPRZ was simulated through computational 3D-modeling for confirmation through the best docking score (−9.513). c) TMZ loading (>1 μg) to produce a nano-awakener was determined using LC-MS/MS with size characterization (average ≈117 nm) by transmission electron microscopy imaging (scale bar = 100 nm). d) The superior targeting efficiency of PT-displayed CS-NVs (red) to those of liposome and SC or no peptide CS-NVs was indicated by co-localization (gray) with PTTRZ1 (green) in the entire cell area including nucleus (blue), as determined by confocal imaging with quantitative analysis (n = 3, scale bar = 20 μm). Data = mean ± standard deviation. $^{**}p$ <0.01 no peptide versus liposome, $^{**}p$ <0.01 between lined groups and $^{***}p$ < 0.001 between all groups. e) Consequently, the nano-awakener with additional TMZ treatment in the media exerted a stronger anti-cancer effect on CSCs compared with that of no TMZ (CSC-NV-PT-PEG) and only TMZ loading (nano-awakener) (n = 5). Data = mean ± standard deviation. $^{*}p$ <0.05, $^{**}p$ <0.01 versus NV-PT and $^{***}p$ < 0.001 between lined groups.

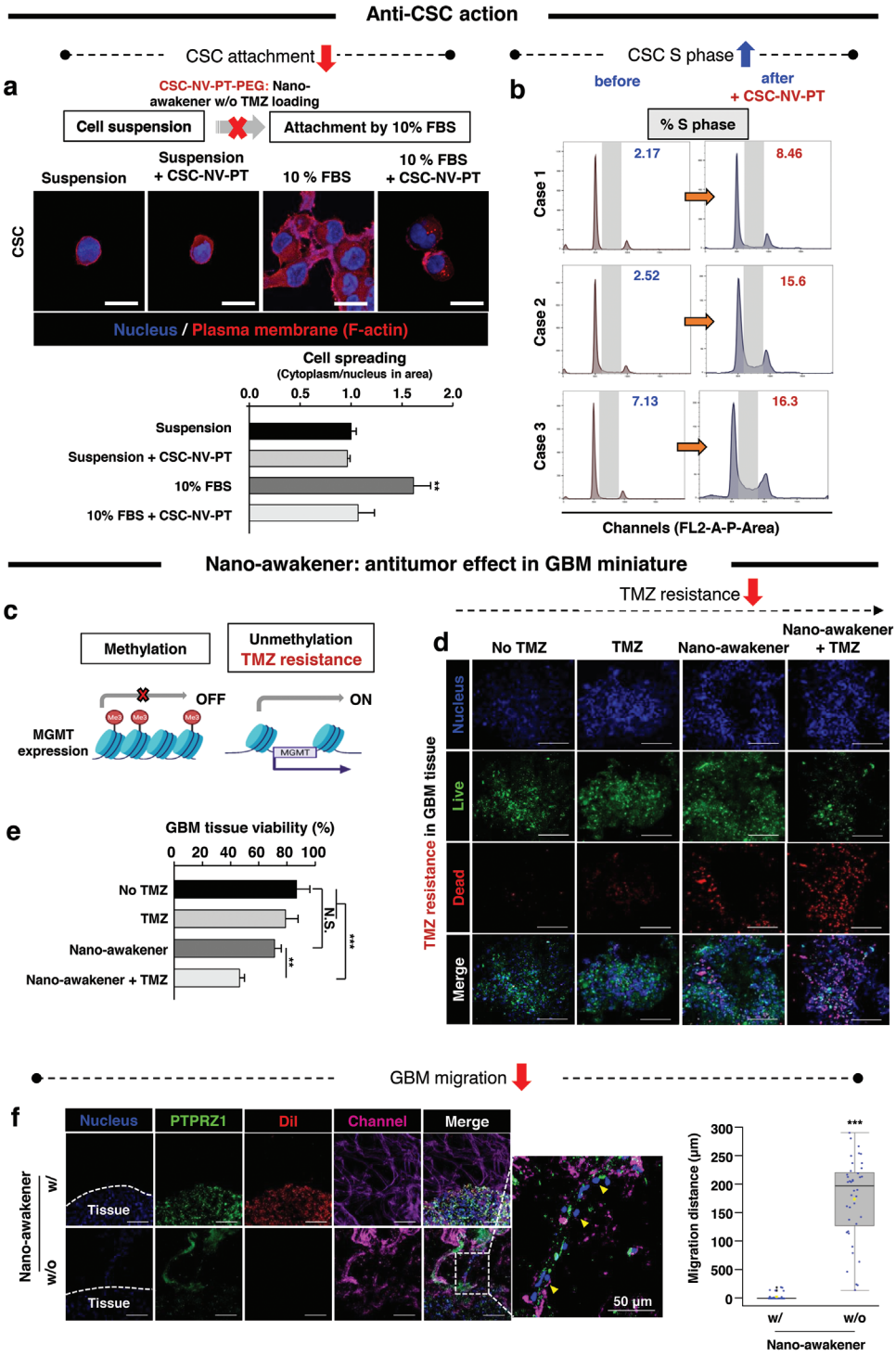

Figure 6. The nano-awakener exerts pro-TMZ effects against CSCs through activation of the S phase process with anti-attachment function. a) Treatment of CSC-WT-PT-PEG (nano-awakener without TMZ loading) for 3 days significantly suppressed the pro-attachment effect of 10% FBS on CSCs to the levels of the suspension groups, as determined by confocal imaging (blue-nucleus and red-plasma membrane) with quantitative analysis ($n = 5$). The cell spreading area was normalized to that of the suspension group. $^{**}p < 0.01$, versus the other groups. b) CSCs were isolated from three cases (1–3) of GBM miniature using patient samples. Treatment with CSC-WT-PT-PEG for 3 days induced the S phase process (2–6 times), making CSCs susceptible to TMZ, as analyzed by flow cytometry using PI (DNA content dye). c) As unmethylation of the MGMT promoter promotes drug resistance in cancer cells, nano-awakener treatment was expected to alter this status and thereby make CSCs susceptible to TMZ. d) When additional TMZ was added to the media, the anti-CSC effects of nano-awakener treatment in a 3-day culture resulted in the highest CSC death among the test groups, as determined by the live(green)/dead(red) assay (blue: nucleus), e) which was also confirmed by quantitative image analysis of tissue viability ($n = 3$, scale bar = 200 μm). $^{**}p < 0.01$, $^{***}p < 0.001$ between lined groups (N.S.: no significance). f) Owing to the anti-attachment effect and the induction of the S phase

susceptible to TMZ. These results validate the therapeutic actions of nano-awakeners, specifically those targeting GBM CSCs.

As unmethylation of the MGMT promoter promotes drug resistance in cancer cells (Figure 6c), nano-awakener treatment was expected to alter this status, thereby making CSCs susceptible to the anticancer effects of TMZ. As a validation point, when additional TMZ was added to the media, the anti-CSC effects of nano-awakener treatment during the 3-day culture promoted CSC death most effectively among the tested treatments (Figure 6d,e). Owing to the targeting function with the induction of anti-attachment and anti-quiescence (Figure 6f), the nano-awakener targeted PTPRZ1$^+$GBM cells specifically and suppressed cell migration through the channel network for a 14-day culture in the GBM miniature. In contrast, the absence of a nano-awakener (without group) allowed PTPRZ1$^+$ CSCs to migrate along channels away from the tissue origin, indicating the promising potential of nano-awakeners in suppressing GBM recurrence.

3. Discussion

GBM is a fast-growing brain tumor that causes high mortality, raising the urgent need to reinforce the current therapeutic paradigm. One of the reasons why GBM therapy is challenging is that GBM diffuses aggressively from its origin (e.g., subventricular zone) to other parts (e.g., cerebral parenchyma) of the brain.[11] This diffusive characteristic of GBM attenuates the drug effect, thereby providing a chance for GBM to gain recurrence potential. CSCs are known to migrate from the tumor mass by sidestepping anticancer treatments, leading to cancer recurrence.[12] In this study, GBM miniature enabled the elucidation and proof of this mechanism via monitoring of time-dependent changes in the genetic and cellular signatures of GBM tissue by allowing efficient cell migration through microchannels as a route guidance. This advantage was provided by recapturing of the GBM niche factors (associated cells, ECM, and microchannels) together in one system, which allows for the maintenance of their temporal and spatial changes in a vital fashion. Moreover, the drug responsiveness of GBM patient tissue in the GBM miniature was aligned with the clinical outcomes even when tested within 1 day post-culture, representing a promising option to aid prompt and accurate clinical decisions in foreseeing patient-specific prognosis. As needed, the number of chips can be increased in a single operation, in contrast to the time-consuming process of a one-by-one clinical decision. These game-changing functions cannot be applied without a direct tissue culture system.

Each GBM tissue exhibited patient-specific variations in tissue characteristics,[1] which might alter the responses of GBM miniature in a case-by-case manner. Hence, the consistency of each tissue reaction was improved by punching peripheral tissues into thin pieces (1 mm): i) to avoid disruption of tissue composition and structure, as seen in a thick piece; ii) to exclude a hypoxic central mass containing dead cells; and thus, iii) to include active GBM cells that migrated to the peripheral areas. The size homogeneity of the tissue piece was relied on for the size of the 1-mm-diameter biopsy punch.

As a standard anticancer drug for GBM treatment, TMZ disturbs DNA synthesis and the consequent cell cycle process, thereby inducing cancer cell death. However, when cancer cells are in the quiescent (G0) phase, they do not require DNA synthesis and thus escape the anticancer effect of TMZ, allowing for the diffusive migration of quiescent cells from the origin to other areas. PTPRZ1 was chosen as a target molecule for CSC-NVs with peptide display, as overexpression of PTPRZ1 was observed in migratory GBM cells accompanying stemness markers with a build-up of cancer malignancy.[13] The results showed that the binding of the displayed peptide to PTPRZ1 awakened GBM stem cells (G0 phase) and inhibited their attachment and migration, leading to cell death upon additional treatment with soluble TMZ, which represents a punchline strategy based on the concept of one shot-multiple kills. As the efficient binding of the displayed peptide with PTPRZ1 was the main player in this strategy, the peptide sequence was confirmed in silico to have a higher docking score and Emodel values than the scramble control, indicating that this tool is beneficial for advancing the design of nanotherapy. Together, the design strategy and functional validation in this nanotherapy serve as a breakthrough model of the mechanism-learned approach, thereby innovating the therapeutic paradigm of GBM medicine.

As items for future studies, the potential of the GBM miniature to help clinicians predict the prognosis of patient-specific therapeutic choices needs to be tested in a clinical context. This process may require a pre-investigation of the patient's background in association with subsequent drug resistance. Hence, whether drug screening in GBM miniatures can preserve and reflect patient-specific epigenetic alterations should be investigated in future studies. In addition, testing new drugs or new combinations of existing drugs will add validation power to improve the functional credibility of the GBM miniature. Moreover, the effect of the PTPRZ1-nanovesicle needs to be tested in vivo upon implantation of a GBM miniature into the brain. The efficiency of local versus intravenous injections should be compared to suggest a treatment method and to provide related mechanistic insights for translation.

4. Experimental Section

Glioblastoma Patient Tissue, Cell Spheres, Culture Media, Cryopreservation, and Viability: Upon agreement with each patient, glioblastoma (GBM) tissues were harvested during surgery to remove tumor masses according to the procedures and guidelines approved by the Institutional Committee of Yonsei University College of Medicine (IRB 4-2012-0212, 4-2021-1319). The harvested tissues were transferred to the laboratory on ice within a few hours. Each GBM tissue sample was punched into pieces using a 1-mm-diameter biopsy punch (BP-10F; Kai Medical, TX, USA). As reported previously,[14] cell spheres (CS) were produced by: i) physically

process, the nano-awakener (red) targeted PTPRZ1$^+$GBM cells (green) and suppressed cell migration through the channel network (pink) in a 14-day culture in the GBM miniature. In contrast, migratory PTPRZ1$^+$ CSCs (yellow arrow) were observed along channels away from the tissue origin in the absence of the nano-awakener (without group), as determined by immunostaining with confocal imaging and quantitative image analysis ($n = 4$). ***p <0.001 versus with and without nano-awakener. Data = mean ± standard deviation.

dissociating patient tissues with a scalpel; ii) passing them through a cell strainer with a nylon mesh (100 µm in diameter) to collect single cells; and iii) culturing to induce self-aggregation into CS in the media (see below).

Samples were cultured in DMEM/F-12 50/50, 1X (Dulbecco's modified Eagle's medium/Ham's F-12 50/50 mixed with L-glutamine) supplemented with 1% Active Ingredient (15140-122; Gibco, Carlsbad, CA, USA), 1× B27 (17504-044; Gibco), 20 ng mL^{-1} epithelial growth factor (PHG0311; Thermo Fisher Scientific, Waltham, MA, USA), and basic fibroblast growth factor (100-18C; PeproTech, Rocky Hill, NJ, USA). For cryopreservation, each tissue sample (20 pieces) was first mixed with 1 mL of cryostor solu-tion (CS10; StemCell, Vancouver, BC, Canada) in a cell stock vial, stored in a frozen container overnight at −70 °C, and then moved to liquid nitrogen. The sample viability was determined by live/dead assay (L3224; Thermo Fisher Scientific) with confocal imaging (LSM 980; Zeiss, Oberkochen, Germany) and quantitative image analysis. Channels were visualized by perfusing a dark-red fluorescence staining solution (1:250 ratio, F10720; Thermo Fisher Scientific) with confocal imaging.

Chip Culture: Microchannel networks were generated inside a gelatin hydrogel to culture GBM tissue pieces (GBM miniature) or CS. As sacrificing structural materials to generate the channel networks, PNIPAM ($M_n \approx 40000$, 535 311; Sigma-Aldrich, St. Louis, MO, USA) fibers were produced by operating a custom-made spinning device with PNIPAM in MeOH solution (53% w/v). The diameter of the PNIPAM fibers was controlled by adjusting the rotational speed (2500–2800 rpm) of the spinning device.[5a,b] The fibers were embedded in a PDMS mold at a density of 11.45 ± 3.13 µg mm^{-3}, and a silicone tube was then placed to connect with the network channel at the inlet and outlet sides. Thus, a closed circulation system was generated so that the culture media could flow from the inlet silicone tube to the channel network and finally into the outlet tube in the circulation. Next, patient tissue (20 mg) was punched to 10 pieces using a biopsy punch or cell spheres were embedded in gelatin (G1890; Sigma-Aldrich) solution at a ratio of 9:1 and mixed with microbial transglutam-inase (mTG, 1201–50; Modernist Pantry LLC, Eliot, ME, USA). The sam-ple mixture was poured onto the fibers and subjected to gelation by mTG cross-linking at 37 °C for 30 min, thereby positioning each sample in the chip. The PNIPAM fibers were then dissolved by sol-gel transition at room temperature (RT) using PBS.[5c,9,15] The GBM miniature cells were cul-tured by perfusing the culture media at a flow rate of 20 µL min^{-1} through a microchannel network. The test culture systems included 2D tissue cul-ture polystyrene (2D TCPS), gelatin gel without (static without channel) or with channel networks in perfusion-free culture (static with channel), and GBM miniature with channels and perfusion culture using a peristaltic pump.

RNA Sequencing: RNA sequencing data were analyzed by processing the raw fastq files with a Linux pipeline[16] and calculating the initial set of expression in units of fragments per kilobase million (FPKM). The unpaired reads were removed using Trimommatic 0.39 (TruSeq3-PE-2. fa min length of 50),[17] and the paired reads were aligned on the human chromo-some GRCh38.84 through hisat2 (Version 2.1.0).[18] The data were sorted using samtools (Version 1.12)[19] and passed to the stringtie (Version 2.0.6) for gtf construction.[20] All GTF data were merged and recalculated into new data, and the FPKM was determined using ballgown (version 2.26.0).[21] Next, the gene set and copy number variations (CNV) were analyzed using the corresponding FPKM and subsequent TPM values as follows:

For the analysis of gene set variation, a scoring system was used to pre-dict the enrichment of a specified gene list in each RNA sequencing sam-ple. All transcript-level FPKM values were compiled into specified gene names for scoring without excluding any genes, and the raw expression dataset was processed without modifications. The GSVA algorithm (Ver-sion 1.42.0) was used to score each sample with the gene lists after compil-ing the Hugo gene symbols from Ensembl,[22] followed by the calculation of scores increasing from 0 to the maximum difference through a random walk process. Each sample was validated by analyzing CNV and ruling out the possibility of culturing erroneous cell types using the algorithm from the authors' previous study.[23] As cancer cells and fibroblasts may com-pete in the culture process, the CNV of cell chromosomes was analyzed as a validation method to prevent the misclassification of samples.[24] As cancer cells harbor cancer-specific CNV patterns, chromosome 7 gain and chromosome 10 loss were used as chromosome-level markers of brain tumors.[25]

GBM Patient Survival Rates in Clinical Settings: The treatment efficacy of the early anticancer drug Active Ingredient (TMZ) after surgery was determined by plotting the Kaplan–Meier curve using the survival package (version 3.2–13) and the ggpubr package (version 0.4.0).[10,26] Clinical cohort data were used from the TMZ perspective. Patients without any medical history in the electronic medical record system were excluded from analysis. GBM patients with wild-type isocitrate dehydrogenase (IDH) were examined by classifying them into two groups: those treated with TMZ earlier or later than 15 days after surgery.

TMZ, Irradiation, or Nanovesicle (NV) Treatment: As representative therapeutic options for GBM treatment, TMZ (T2577; Sigma-Aldrich) and irradiation at 3 Gy using an X-Rad 320 (Precision X-Ray, Madison, CT, USA) were administered to CS in either the TCPS or the chip and GBM miniature ($n = 3$). For CS in TCPS, the spheres were collected by centrifugation at 200 × g for 3 min, followed by dissociation of each pellet into single cells after incubation in Accutase (A1110501; Thermo Fisher Scientific) solution for 2 min, as reported previously.[16] Cells were seeded at 1 × 10^4 cells/well overnight in a culture medium in 96-well plates. For testing in the chip, CS (1 × 10^6) or GBM tissue pieces were cultured for one day. The samples in each well were then treated with TMZ (250 µM) or irradiated with 3 Gy X-Rad 320 for 72 h.

The cytotoxic effects of CSC-NV (0, 40, 80, 160 µg mL^{-1}) on CSCs (2 × 10^4/well in a 96-well plate) were determined using the Cell Counting Kit-8 (CCK-8) assay (1:10 ratio; Dojindo Molecular Technologies, Inc., Rockville, MD, USA). After reading the absorbance at 450 nm using VERSA max (Softmax pro6.2.2; Molecular Devices, San Jose, CA, USA), the corresponding fold change was calculated in comparison with a vehicle (dimethyl sulfoxide) control using Prism 7 software (GraphPad, San Diego, CA, USA).

Immunofluorescence Staining: Samples were fixed with 4% paraformaldehyde (PFA) in PBS at RT for 1 h and washed thrice with PBS. Suspended CSCs were fixed with a mixture of methanol and acetic acid (3:1 ratio) at RT for 3 min and washed with PBS three times. The samples were permeabilized using PBS containing 0.2% Triton X-100 (X100; Sigma-Aldrich) at RT for 1 h, followed by three PBS washes. The samples were then blocked with PBS containing 0.1% Tween-20 (P9416; Sigma-Aldrich), 1% bovine serum albumin (BSA), and 0.3 M glycine at RT for 2 h. Next, the samples were incubated with mouse monoclonal anti-Olig2 antibody (1:200, MA5-15810; Thermo Fisher Scientific), rabbit polyclonal anti-PTP zeta antibody (1:250, ab126497; Abcam, Cambridge, MA, USA), and rabbit polyclonal anti-CD133 antibody (1:100, ab19898; Abcam) at 4 °C overnight. After washing with PBS three times, the samples were incubated with secondary antibodies at a 1:250 dilution, including fluorescein (FITC)-conjugated AffiniPure goat anti-mouse IgG (115-095-003; Jackson Immuno Research, West Grove, PA, USA) for Olig2, as well as Alexa Fluor 594-conjugated AffiniPure goat anti-rabbit IgG (111-585-003; Jackson Immuno Research) for CD133, at RT for 2 h, followed by washing three times in PBS.

The anti-attachment effect of CSC-NV-PT-PEG (nano-awakener without TMZ:0, 40, 80, 160 µg mL^{-1}) on CSCs was examined in DMEM/F-12 50/50, 1× complement medium, followed by the addition of 10%FBS/1% Active Ingredient on day 3 post-culture. The cells were fixed with a mix-ture of methanol/acetic acid for 3 min and washed thrice with PBS. The plasma membrane was stained with rhodamine solution (1:250, R415; Thermo Fisher), nuclei were counterstained with DAPI, and channels were stained using an orange fluorescence staining solution (1:250 ra-tio, F10720; Thermo Fisher), followed by confocal imaging. After selecting Olig2$^+$/CD133$^+$ cells around the channels, cell migration from the tissue origin (cell type and distance), and cytosol-to-nucleus ratio in the area were analyzed using Imaris 7.3 (Bitplane, Belfast, GBR).

The efficiency of CSC-NV-PT-PEG in targeting CSCs was examined by labeling the NV test groups with Vybrant DiI cell-labeling solution (1:250, V22885; Thermo Fisher) for 30 min, followed by centrifugation at 14 800 rpm for 30 min to remove the supernatant solution. The NV groups (160 µg mL^{-1}) were treated with CSCs for three days, and PTPRZ1 was

immunoblotted with DAPI nuclear staining in a mounting medium. The samples were then subjected to confocal microscopy.

Flow Cytometry: The expression of CSC (PTPRZ1, Olig2, CD133, and Oct3/4) and glial cell (GFAP) markers was characterized by flow cytometry (BD FACS Verse II; BD Bioscience, CA, USA) with quantitative analysis. Cells (1×10^6) were fixed in a cold methanol solution (100%) at −20 °C for 10 min, centrifuged, and washed twice in PBS with 1% bovine serum albumin (BSA) solution. The cells were then treated with rabbit polyclonal anti-PTP zeta (1:200, ab126497; Abcam), mouse monoclonal anti-Olig2 (1:500, MA5-15810; Thermo Fisher), rabbit polyclonal anti-CD133 (1:500, ab19898; Abcam), rabbit polyclonal anti-GFAP (1:250, ab7260; Abcam), and mouse monoclonal Oct3/4 (1:200, sc-5279; Santa Cruz Biotechnology, CA, USA). The samples were treated with secondary antibodies (1:500) of fluorescein isothiocyanate (FITC)-conjugated AffiniPure goat anti-mouse IgG for Olig2, Oct3/4 and Alexa Fluor 594-conjugated AffiniPure goat anti-rabbit IgG for PTPRZ1, CD133 and GFAP at RT for 1 h.

The "wake-up" effect of the nano-awakener to activate the cell cycle progression of CSCs was then examined by harvesting CSCs post-migration in the GBM miniature. CSCs were washed in cold PBS, fixed in a cold 70% EtOH solution for 30 min at 4 °C, washed twice in the PBS solution, and centrifuged at 850 × *g* for 3 min to remove the EtOH solution. The samples were incubated with ribonuclease solution (100 µg mL^{-1}, R6513; Sigma-Aldrich) for 15 min at 37 °C with propidium iodide solution (50 µg mL^{-1}, P4864; Sigma-Aldrich).

Liposome Production: Liposomes were prepared using a rapid injection method. Briefly, 1,2-dipalmitoyl-sn-glycero-3-phosphocholine (DPPC; 850355P, Sigma-Aldrich, MO, USA), cholesterol (C8667, Sigma-Aldrich), and 1,2-distearoyl-sn-glycero-3-phosphoethanolamine-N-[methoxy(polyethylene glycol)-2000] (DSPE-mPEG; 880120P, Sigma-Aldrich) were dissolved (55:40:5 molar ratio) in ethanol (E7023, Sigma-Aldrich) at 72 °C to a final concentration of 200 mmol L^{-1}. The mixtures were rapidly injected into the same volume of PBS using a 20-gauge needle (Koreavaccine, Seoul, Republic of Korea) with vigorous stirring (500 rpm) at 72 °C, followed by vigorous stirring for 15 min. Next, the liposome mixture was extruded through a stack of three filters as a sequential overlap setting of the drain disc (PETEDD9025, Sterlitech, WA, USA), 0.1 µm membrane filter (PCT019030, Sterlitech), and drain disc again at 25 mL min^{-1} using an extruder (GOE-1000 mL, Genizer, CA, USA) with peristaltic pumping (BT100L, Lead Fluid Technology, Heibei, China).

CSC-NV Production: CSCs were collected by centrifugation at 1300 rpm for 3 min and suspended in PBS (4 mL) after treatment with a debris removal solution (1 mL, 130-109-398; Miltenyi Biotec Inc., GL, DEU). The samples were then centrifuged at 3000 × *g* for 10 min and the intermediate debris phase was removed, followed by the addition of PBS (15 mL) and centrifugation at 1000 × *g* at 4 °C for 10 min. NVs were produced by perfusing the cell suspension through a series of membrane filters (Sterlitech, Auburn, WA, USA) with decremental pore sizes from 10 to 5 and to 0.1 µm using a peristaltic pump at 25 mL min^{-1}. NVs were collected by centrifugation at 14 000 rpm for 30 min and their concentrations were determined using a BCA protein assay kit (23 227; Thermo Fisher).

Nano-Awakener Production: As a functional blocker, the sequence of the peptide to target PTPRZ1 (PT) was determined as KAKPSPQEK in contrast to the scramble control (SC: KPKPQAESK) through computer modeling of peptide-PTPRZ1 binding by calculation of each docking score using the Schrodinger software suite (Schrodinger Release 2021-1; Maestro. Schrodinger, NY, USA). The 3D structures of the peptide and PTPRZ1 were obtained from the RCSB Protein Data Bank (PDB).[27] Next, PT and SC were synthesized from an outsourcing service (LugenSci, Seoul, Republic of Korea). The peptide was conjugated to polyethylene glycol (PEG) using *N*-(3-dimethylaminopropyl)-*N*-ethylcarbodiimide hydrochloride (E7750; Sigma-Aldrich) by reacting peptide-NH_2 with COOH-PEG2000-DSPE (880135P; Sigma-Aldrich) at a molar ratio of 1:1 with stirring for 24 h at RT. As the first removal process, unreacted DSPE-PEG2000-COOH and peptide were filtered through a dialysis tube (MWCO = 3.5 kDa, G235003; Spectrum Lab, Piraeus, Greece). As the second removal process, the filtering product (10% w/w) was electrically disturbed with two cycles of pulse (1400 V for 2 ms) in a Neon electroporation system (MPK5000; Thermo Fisher). Unreacted peptide and PEG were filtered using a dialysis tube (MWCO = 20 kDa, G235057; Spectrum Lab), followed by centrifugation at 14800 rpm for 30 min. Finally, a nano-awakener was produced by loading TMZ (500 µM mL^{-1}) into CSC-NV-PT-PEG (1 mg) through electroporation with two pulse cycles (1400 V for 2 ms) in the Neon electroporation system. Unreacted peptides with TMZ were filtered through a dialysis tube (MWCO = 20 kDa), followed by centrifugation at 14 800 rpm for 30 min.

Nano-Awakener Characterization: The morphology and size were analyzed using transmission electron microscopy (TEM) (Jem2100; JEOL, Tokyo, Japan). FTIR spectroscopy (Nicolet 6700; Thermo Fisher Scientific) was used to confirm successful step-by-step conjugation: i) peptide to PEG (PT or SC-PEG) with major peaks at 1765 cm^{-1} (C=O stretching vibration); and ii) PT or SC-PEG to CSC-NV with sharper bands at 1765 and 1600 cm^{-1} (C=O and N–H stretching vibration, respectively). TMZ loading to CSC-NV-PT-PEG was determined using LC/MS (xcalibur v. 4.0; Thermo Fisher) with concentration calculations against a TMZ standard curve.

Statistical Analysis: Data were analyzed using Excel and SigmaPlot 12.0 (Systat Software Inc., San Jose, CA, USA) and Prism 7. Data are presented as the means ± standard error of the mean from at least three independent experiments. A two-tailed Student's *t*-test was used for paired comparisons, and a one-way ANOVA with Tukey's significant difference post-hoc test was applied for multiple comparisons. Values of * $p < 0.05$, ** $p < 0.01$, and *** $p < 0.001$ were considered statistically significant. The sample sizes (*n*) are presented in the corresponding sections. Data normalization and transformation are shown in the corresponding figure legends.

Supporting Information

Supporting Information is available from the Wiley Online Library or from the author.

Acknowledgements

S.-J.Y., S.B., and S.E.Y. contributed equally to this work. This work was supported by the Korea Medical Device Development Fund grant funded by the Korea government (the Ministry of Science and ICT, the Ministry of Trade, Industry and Energy, the Ministry of Health & Welfare, the Ministry of Food and Drug Safety (Project Number:1711138302, KMDF_PR_20200901_0152-01), and the Bio & Medical Technology Development Program of the National Research Foundation (NRF-2019R1A2C2010802) to H.J.S. National Research Foundation of Korea (NRF) grants funded by the Korea government (MSIT) (NRF-2022R1A2B5B03001199), the Ministry of Science and ICT (NRF-2020M2D9A2092372), the Bio & Medical Technology Development Program of the National Research Foundation (NRF) funded by the Ministry of Science & ICT (NRF-2020M3E5E2037960), and the "Team Science Award" of Yonsei University College of Medicine (6-2021-0192) to S.G.K. Figure illustrations were created with BioRender.com.

Conflict of Interest

The authors declare no conflict of interest.

Data Availability Statement

The data that support the findings of this study are available from the corresponding author upon reasonable request.

Keywords

drug response, glioblastoma patient-tissue chip culture, nanotherapy, PTPRZ1, RNA sequencing

Received: July 3, 2022
Revised: August 12, 2022
Published online: September 1, 2022

[1] a) J. A. Joyce, J. W. Pollard, *Nat. Rev. Cancer* **2009**, *9*, 239; b) T. C. Steed, J. M. Treiber, K. Patel, V. Ramakrishnan, A. Merk, A. R. Smith, B. S. Carter, A. M. Dale, L. M. Chow, C. C. Chen, *Oncotarget* **2016**, *7*, 24899.

[2] a) A. R. Pine, S. M. Cirigliano, J. G. Nicholson, Y. Hu, A. Linkous, K. Miyaguchi, L. Edwards, R. Singhania, T. H. Schwartz, R. Ramakrishna, D. J. Pisapia, M. Snuderl, O. Elemento, H. A. Fine, *Cancer Discovery* **2020**, *10*, 964; b) H. G. Yi, Y. H. Jeong, Y. Kim, Y. J. Choi, H. E. Moon, S. H. Park, K. S. Kang, M. Bae, J. Jang, H. Youn, S. H. Paek, D. W. Cho, *Nat. Biomed. Eng.* **2019**, *3*, 509; c) A. Sontheimer-Phelps, B. A. Hassell, D. E. Ingber, *Nat. Rev. Cancer* **2019**, *19*, 65.

[3] a) R. A. Burrell, N. McGranahan, J. Bartek, C. Swanton, *Nature* **2013**, *501*, 338; b) G. P. Dunn, M. L. Rinne, J. Wykosky, G. Genovese, S. N. Quayle, I. F. Dunn, P. K. Agarwalla, M. G. Chheda, B. Campos, A. Wang, C. Brennan, K. L. Ligon, F. Furnari, W. K. Cavenee, R. A. Depinho, L. Chin, W. C. Hahn, *Genes Dev.* **2012**, *26*, 756.

[4] R. Stupp, W. P. Mason, M. J. van den Bent, M. Weller, B. Fisher, M. J. B. Taphoorn, K. Belanger, A. A. Brandes, C. Marosi, U. Bogdahn, J. Curschmann, R. C. Janzer, S. K. Ludwin, T. Gorlia, A. Allgeier, D. Lacombe, J. G. Cairncross, E. Eisenhauer, R. O. Mirimanoff, *N. Engl. J. Med.* **2005**, *352*, 987.

[5] a) J. M. Oh, C. C. Venters, C. Di, A. M. Pinto, L. Wan, I. Younis, Z. Cai, C. Arai, B. R. So, J. Duan, G. Dreyfuss, *Nat. Commun.* **2020**, *11*, 1; b) J. B. Lee, X. Wang, S. Faley, B. Baer, D. A. Balikov, H. J. Sung, L. M. Bellan, *Adv. Healthcare Mater.* **2016**, *5*, 781; c) S. Baek, S. E. Yu, Y. H. Deng, Y. J. Lee, D. G. Lee, S. Kim, S. Yoon, H. S. Kim, J. Park, C. H. Lee, J. B. Lee, H. J. Kong, S. G. Kang, Y. M. Shin, H. J. Sung, *Adv. Healthcare Mater.* **2022**, *11*, 2102226.

[6] a) M. N. Vu, H. G. Kelly, A. K. Wheatley, S. Peng, E. H. Pilkington, N. A. Veldhuis, T. P. Davis, S. J. Kent, N. P. Truong, *Small* **2020**, *16*, 2002861; b) S. Y. Khor, M. N. Vu, E. H. Pilkington, A. P. Johnston, M. R. Whittaker, J. F. Quinn, N. P. Truong, T. P. Davis, *Small* **2018**, *14*, 1801702.

[7] J. S. Rao, *Nat. Rev. Cancer* **2003**, *3*, 489.

[8] T. A. Ulrich, E. M. de Juan Pardo, S. Kumar, *Cancer Res.* **2009**, *69*, 4167.

[9] H. J. Yoon, Y. S. Chung, Y. J. Lee, S. E. Yu, S. Baek, H. S. Kim, S. W. Kim, J. Y. Lee, S. Kim, H. J. Sung, *Adv. Sci.* **2021**, *8*, 2102640.

[10] J. H. Lee, J. E. Lee, J. Y. Kahng, S. H. Kim, J. S. Park, S. J. Yoon, J. Y. Um, W. K. Kim, J. K. Lee, J. Park, E. H. Kim, J. H. Lee, J. H. Lee, W. S. Chung, Y. S. Ju, S. H. Park, J. H. Chang, S. G. Kang, J. H. Lee, *Nature* **2018**, *560*, 243.

[11] J. Chen, Y. Li, T. S. Yu, R. M. McKay, D. K. Burns, S. G. Kernie, L. F. Parada, *Nature* **2012**, *488*, 522.

[12] a) Z. Xia, D. Ouyang, Q. Li, M. Li, Q. Zou, L. Li, W. Yi, E. Zhou, *J. Cancer* **2019**, *10*, 1663; b) S. Müller, P. Kunkel, K. Lamszus, U. Ulbricht, G. A. Lorente, A. M. Nelson, D. von Schack, D. J. Chin, S. C. Lohr, M. Westphal, T. Melcher, *Oncogene* **2003**, *22*, 6661; c) M. Nishita, S. Y. Park, T. Nishio, K. Kamizaki, Z. Wang, K. Tamada, T. Takumi, R. Hashimoto, H. Otani, G. J. Pazour, V. W. Hsu, Y. Minami, *Sci. Rep.* **2017**, *7*, 1.

[13] a) T. Bae, L. Tomasini, J. Mariani, B. Zhou, T. Roychowdhury, D. Franjic, M. Pletikos, R. Pattni, B. J. Chen, E. Venturini, B. Riley-Gillis, N. Sestan, A. E. Urban, A. Abyzov, F. M. Vaccarino, *Science* **2018**, *359*, 550; b) H. Y. Kim, B. I. Lee, J. H. Jeon, D. K. Kim, S.-G. Kang, J.-K. Shim, S. Y. Kim, S. W. Kang, H. Jang, *Biomolecules* **2019**, *9*, 595.

[14] J. B. Lee, J. S. Park, Y. M. Shin, D. H. Lee, J. K. Yoon, D. H. Kim, U. H. Ko, Y. Kim, S. H. Bae, H. J. Sung, *Adv. Funct. Mater.* **2019**, *29*, 1900075.

[15] S. J. Yoon, H. Y. Son, J. K. Shim, J. H. Moon, E. H. Kim, J. H. Chang, W. Y. Teo, S. H. Kim, S. W. Park, Y. M. Huh, S. G. Kang, *J. Transl. Med.* **2020**, *18*, 482.

[16] A. M. Bolger, M. Lohse, B. Usadel, *Bioinformatics* **2014**, *30*, 2114.

[17] D. Kim, J. M. Paggi, C. Park, C. Bennett, S. L. Salzberg, *Nat. Biotechnol.* **2019**, *37*, 907.

[18] H. Li, B. Handsaker, A. Wysoker, T. Fennell, J. Ruan, N. Homer, G. Marth, G. Abecasis, R. Durbin, *Bioinformatics* **2009**, *25*, 2078.

[19] S. Kovaka, A. V. Zimin, G. M. Pertea, R. Razaghi, S. L. Salzberg, M. Pertea, *Genome Biol.* **2019**, *20*, 278.

[20] A. C. Frazee, G. Pertea, A. E. Jaffe, B. Langmead, S. L. Salzberg, J. T. Leek, *Nat. Biotechnol.* **2015**, *33*, 243.

[21] a) R. J. Kinsella, A. Kähäri, S. Haider, J. Zamora, G. Proctor, G. Spudich, J. Almeida-King, D. Staines, P. Derwent, A. Kerhornou, P. Kersey, P. Flicek, *Database* **2011**, *2011*, bar030; b) S. Hänzelmann, R. Castelo, J. Guinney, *BMC Bioinformatics* **2013**, *14*, 7.

[22] A. P. Patel, I. Tirosh, J. J. Trombetta, A. K. Shalek, S. M. Gillespie, H. Wakimoto, D. P. Cahill, B. V. Nahed, W. T. Curry, R. L. Martuza, D. N. Louis, O. Rozenblatt-Rosen, M. L. Suvà, A. Regev, B. E. Bernstein, *Science* **2014**, *344*, 1396.

[23] a) S. E. Hooker, L. Woods-Burnham, M. Bathina, S. Lloyd, P. Gorjala, R. Mitra, L. Nonn, K. S. Kimbro, R. A. Kittles, *Cancer Epidemiol., Biomarkers Prev.* **2019**, *28*, 1003; b) A. de Weck, H. Bitter, A. Kauffmann, *bioRxiv* **2017**, 166199.

[24] a) M. Gerstung, C. Jolly, I. Leshchiner, S. C. Dentro, S. Gonzalez, D. Rosebrock, T. J. Mitchell, Y. Rubanova, P. Anur, K. Yu, M. Tarabichi, A. Deshwar, J. Wintersinger, K. Kleinheinz, I. Vázquez-García, K. Haase, L. Jerman, S. Sengupta, G. Macintyre, S. Malikic, N. Donmez, D. G. Livitz, M. Cmero, J. Demeulemeester, S. Schumacher, Y. Fan, X. Yao, J. Lee, M. Schlesner, et al., *Nature* **2020**, *578*, 122; b) V. Körber, J. Yang, P. Barah, Y. Wu, D. Stichel, Z. Gu, M. N. C. Fletcher, D. Jones, B. Hentschel, K. Lamszus, J. C. Tonn, G. Schackert, M. Sabel, J. Felsberg, A. Zacher, K. Kaulich, D. Hübschmann, C. Herold-Mende, A. von Deimling, M. Weller, B. Radlwimmer, M. Schlesner, G. Reifenberger, T. Höfer, P. Lichter, *Cancer Cell* **2019**, *35*, 692.

[25] M. T. Terry, M. G. Patricia, *Modeling Survival Data: Extending the Cox Model*, Springer, New York **2000**.

[26] S. J. Yoon, J. Noh, H. Y. Son, J. H. Moon, E. H. Kim, S. W. Park, S. H. Kim, J. H. Chang, Y. M. Huh, S. G. Kang, *Cancer Med.* **2020**, *9*, 9018.

[27] H. M. Berman, J. Westbrook, Z. Feng, G. Gilliland, T. N. Bhat, H. Weissig, I. N. Shindyalov, P. E. Bourne, *Nucleic Acids Res.* **2000**, *28*, 235.